Chemosphere 361 (2024) 142539

Contents lists available at ScienceDirect

Chemosphere

journal homepage: www.elsevier.com/locate/chemosphere

Removal of trivalent chromium ions in model contaminated groundwater using hexagonal boron nitride as an adsorbent

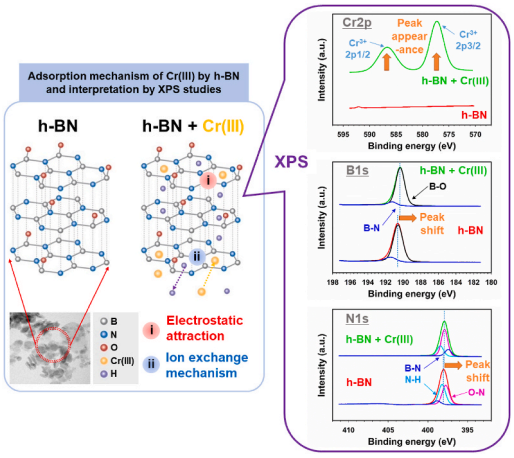
Byung-Moon Jun [a], Deokhwan Kim [b,c], Jaegwan Shin [d], Kangmin Chon [d,e], Chanhyuk Park [f], Hojung Rho [b,c,*]

[a] Radwaste Management Center, Korea Atomic Energy Research Institute (KAERI), 111 Daedeok-Daero 989beon-gil, Yuseong-Gu, Daejeon, 34057, Republic of Korea
[b] Department of Environment Research, Korea Institute of Civil Engineering and Building Technology (KICT), 283 Goyang-Daero, Ilsanseo-Gu, Goyang-si, Gyeonggi-do, 10223, Republic of Korea
[c] Department of Civil and Environment Engineering, University of Science and Technology (UST), 217 Gajeong-Ro, Yuseong-Gu, Daejeon, 34113, Republic of Korea
[d] Department of Integrated Energy and Infra system, Kangwon National University, 1, Kangwondaehak-gil, Chuncheon-si, Gangwon-do, 24341, Republic of Korea
[e] Department of Environmental Engineering, College of Engineering, Kangwon National University, 1, Kangwondaehak-gil, Chuncheon-si, Gangwon-do, 24341, Republic of Korea
[f] Department of Environmental Science and Engineering, Ewha Womans University, 52 Ewhayeodae-gil, Seodaemun-gu, Seoul, 03760, Republic of Korea

HIGHLIGHTS

- h-BNs, two-dimensional materials, boast a large surface area and high stability.
- Five types of h-BNs were utilized to investigate Cr(III) adsorption mechanism.
- The presence of K and Mg showed minimal impact on Cr(III) adsorption efficiency.
- Humic acid enhanced the adsorption performance of Cr(III) by h-BN.
- h-BN is an effective adsorbent for Cr(III) in groundwater treatment.

GRAPHICAL ABSTRACT



ARTICLE INFO

Handling editor: Veeriah (Jega) Jegatheesan

Keywords:
Boron nitride
Groundwater
Water treatment
Chromium adsorption

ABSTRACT

The feasibility of using hexagonal boron nitride (h-BN) to treat heavy metal Cr(III) from model contaminated groundwater was evaluated in this study by adsorption experiments and characterizations. To the best of our knowledge, this study is the first attempt to conduct the adsorption of Cr(III) by h-BN under various experimental conditions such as exposure time, ratio of adsorbates and adsorbents, solution pH, background ions with different ionic strength, and the presence of humic acids (HA) in model contaminated groundwater. The optimized h-BN showed excellent maximum adsorption capacity (*i.e.*, 177 mg • g^{-1}) when the concentrations of Cr(III) and h-BN

* Corresponding author.
E-mail address: hojungrho@kict.re.kr (H. Rho).

https://doi.org/10.1016/j.chemosphere.2024.142539
Received 11 April 2024; Received in revised form 27 May 2024; Accepted 3 June 2024
Available online 4 June 2024
0045-6535/© 2024 The Authors. Published by Elsevier Ltd. This is an open access article under the CC BY-NC license (http://creativecommons.org/licenses/by-nc/4.0/).

were 10 and 10 mg • L^{-1}, respectively. Subsequently, we confirmed there was a negligible change in the adsorption performance of Cr(III) by h-BN in the presence of co-ions (*i.e.*, K and Mg) in concentrations in a range from 50 to 1000 mg • L^{-1}. Furthermore, the adsorption performance of Cr(III) gradually improved with HA concentrations from 2.5 to 25 mg • L^{-1}. Interestingly, the maximum adsorption performance of Cr(III) by both HA and h-BN increased until 500 mg • g^{-1} in the presence of 25 mg • L^{-1} HA. The adsorption mechanism was clarified by Fourier-transform infrared spectroscopy and X-ray photoelectron spectroscopy. Additionally, we successfully confirmed that h-BN could be reused until five cycles. On the basis of the adsorption performance results and characterizations, h-BN can be utilized as an efficient and practical adsorbent to treat Cr(III) in groundwater treatment.

1. Introduction

Chromium is a general inorganic pollutant with different species of trivalent [Cr(III)] and hexavalent [Cr(VI)] states (Chen et al., 2015). It has been widely utilized in a variety of industrial activities including metallurgy, tanneries, batteries, pharmacy, and electroplating (Li et al., 2014, 2018; Liu et al., 2021). Based on industrialization and urbanization activities in recent year, Cr(VI)-contaminated water has caused severe environmental problems (Huang et al., 2016). Recent research has showed the significance of Cr(III) and Cr(VI) in terms of animal and human health (Monga et al., 2022). Notably, Cr(VI) was classified as a Group 1 carcinogen by The International Agency for Research on Cancer (Manna and Sen, 2024). Even though Cr(VI) is ~500 times more toxic than Cr (III), natural oxidation of Cr(III) to Cr(VI) can take place in lake water as well as field soils (Kumar et al., 2009). For instance, leaching behavior of Cr(VI) into the groundwater by rain causes damage to the environment (Hashem et al., 2024b). Furthermore, the treatment of water containing Cr(III) is thus an important task, because Cr(III) accumulation in edible plants is a potential hazard to the health of both animals and humans (Li et al., 2014; Wang et al., 2021; Petrović et al., 2023). Meanwhile, it is significantly important to determine purification strategies for treatment of various environmental contaminants to the life quality on earth planet (Padervand et al., 2020).

Water incorporating Cr(III) has been treated by physico-chemical and biological methods, including (i) precipitation, (ii) membrane processes, (iii) biotechnology, (iv) electrochemical processes, and (v) adsorption processes (Crini and Lichtfouse, 2019; Liu and Yu, 2021; Lohrentz et al., 2023). Nonetheless, the aforementioned methods to treat water containing Cr(III) have the following critical disadvantages (Crini and Lichtfouse, 2019; Liu and Yu, 2021; Lohrentz et al., 2023; Hashem et al., 2024a, 2024b): (i) precipitation shows non-selective properties for metals and generates large amounts of chemical sludge; (ii) although membrane filtration produces small amounts of solid waste, it requires high energy and maintenance costs; (iii) with biological treatment processes it is very difficult to meet discharge standards for chromium due to the toxicity of Cr; (iv) electrochemical methods require high installation and operating expenses; and (v) regeneration of the used adsorbent is quite expensive in the case of adsorption processes. Among these methods, adsorption processes have been widely applied to treat water containing Cr due to their fast kinetics, low material and operating costs, and ease of operation (Yang et al., 2014; Jun et al., 2019b; Gonsalves and Nemade, 2024).

The high efficiency of adsorption processes is directly correlated to the physico-chemical properties of utilized adsorbents, including (Jun et al., 2019a): (i) high chemical/thermal stability, (ii) large specific surface area, and (iii) easy regeneration. Hexagonal boron nitrides (h-BNs) are ideal candidate adsorbents to treat water including Cr, considering that BN-based adsorbents have been widely utilized to treat heavy metal-contaminated water on the basis of their excellent adsorption efficiencies (Li et al., 2013; Li et al., 2014; Li et al., 2017; Peng et al., 2018; Wang et al., 2018; Bangari et al., 2019; Liu et al., 2019a; Liu et al., 2019b; Oh et al., 2019; Wang et al., 2019; Bangari et al., 2020; Han et al., 2020; Karthikeyan et al., 2020; Kumar et al., 2020; Li et al., 2020; Wang et al., 2020; khan et al., 2021; Chen et al., 2022; Lawal Usman et al., 2022; Song et al., 2023). To the best of our knowledge, nine papers related to the treatment of Cr-contaminated water using BN-based adsorbents have been published (Li et al., 2013, 2014, 2017; Karthikeyan et al., 2020; Kumar et al., 2020; Chen et al., 2022; Lawal Usman et al., 2022; Song et al., 2023; Waheed Kamran et al., 2023). Among them, six studies were related to the treatment of water including Cr(VI) (Karthikeyan et al., 2020; Kumar et al., 2020; Chen et al., 2022; Lawal Usman et al., 2022; Song et al., 2023; Waheed Kamran et al., 2023). Furthermore, in other publications (Li et al., 2013, 2014, 2017), there was a lack of experimental data related to the effect of various background ions (e.g., groundwater conditions) on adsorption performance. In other words, environmental factors in the as-mentioned papers only included solution pH, temperature, and presence of anions. Thus, the present research is the first comprehensive study to clarify the adsorption of Cr(III) by h-BN under various operating conditions [e.g., presence of cations (co-ions) and natural organic matters] from practical and engineering perspectives.

The main purpose of this research is to carry out a systematic investigation of h-BN as an adsorbent for Cr(III) in terms of its adsorption mechanism, based on both adsorption experiments under various groundwater environmental conditions and characterizations [*i.e.*, Fourier-transform infrared spectroscopy (FTIR) and X-ray photoelectron spectroscopy (XPS)]. Specifically, we evaluated the adsorption performance of Cr(III) according to several experimental factors such as exposure time, ratio of adsorbates and adsorbents, solution pH, background ions with different ionic strength, and the presence of humic acids (HA) in model contaminated groundwater. Furthermore, we carried out reusability tests of used h-BN until five cycles to clarify its feasibility from a practical perspective.

2. Materials and methods

2.1. Chemicals and materials

Hydrochloric acid (HCl), potassium chloride (KCl), sodium chloride (NaCl), calcium chloride ($CaCl_2$), magnesium chloride ($MgCl_2$), chromium chloride ($CrCl_3$), sodium hydroxide (NaOH), and humic acid (HA) were obtained from Sigma-Aldrich (St. Louis, Mo, USA). The obtained chemicals were used without further purification for preparation of synthetic groundwater to evaluate adsorption performance. We utilized a general water purifier to prepare all stock solutions in this study (Lee et al., 2023).

2.2. Characterizations of h-BN

Analyses of physico-chemical properties such as crystallinity, surface charge, surface area, surface morphology, and chemical structure were carried out through X-ray diffraction (XRD; D8 Discover, Bruker, Billerica, MA, USA), electrophoresis equipment (ELS-Z1000, Otsuka Electronics, Tokyo, Japan), a porosimeter (Autosorb IQ, Quantachrome, Boynton Beach, FL, USA), scanning electron microscopy/transmission electron microscopy (SEM; S-4800; Hitachi, Tokyo, Japan/TEM; JEM-2100F, JEOL, Tokyo, Japan), and FTIR (Nicolet 6700, Thermo Scientific, Waltham MA, USA), respectively, as clearly explained in our

previous study (Hailemariam et al., 2022; Jun et al., 2024). Furthermore, the adsorption mechanism of Cr on h-BN was clarified by energy-dispersive X-ray spectroscopy (EDS) and XPS (PHI Quantera SXM; ULVAC-PHI, Inc., Osaka, Japan), as referenced from our previous studies (Jun et al., 2020a, 2020b).

2.3. Evaluation of adsorption and desorption properties

The base synthetic groundwater consisted of 50 mg • L^{-1} Na^{+} and Ca^{2+} as representative monovalent and divalent ions to fabricate model groundwater, respectively, taking into consideration previously reported studies (Cruz and Andrade, 2015; Kovalenko et al., 2021; Shiyan et al., 2022; Hansson et al., 2023). The pH of the model groundwater was adjusted by 0.5 M HCl and NaOH stock solution through a pH meter (Orion Star A211, Thermo Scientific, USA). The adsorption capacity of Cr by h-BN at equilibrium (q_e, in mg • g^{-1}) was analyzed by inductively coupled plasma–optical emission spectroscopy (Optima 2100DV, PerkinElmer, UK) (Jun et al., 2019b). The adsorption of Cr by h-BN under various experimental conditions was investigated as follows: (i) a kinetic study as a function of exposure time from 0 to 1440 min, (ii) an isotherm study as a function of equilibrium concentration of Cr (C_e), (iii) studying the effect of solution pH on q_e, (iv) assessing the effect of background ions (i.e., K and Mg) until 1000 mg • L^{-1} on q_e, and (v) evaluating the effect of HA until 25 mg • L^{-1} on q_e. Finally, sequence desorption properties were evaluated to confirm reusability, as referenced from our previous study (Jun et al., 2024).

Several adsorption kinetic models have been utilized to explain the adsorption mechanism. The pseudo-first-order kinetic model is known as proper model for low concentration of solute. The linear form of the pseudo-first-order kinetic model is shown in Eq. (1).

$$\log(q_e - q_t) = \log(q_e) - k_1 t \quad (1)$$

where k_1 is the rate constant for pseudo-first-order kinetic model.

Furthermore, the rate of the pseudo-second order kinetic model (k_2) does not depend on the concentration of the adsorbate, but on the adsorption equilibrium capacity, and the linear form of the kinetic equation is described in Eq. (2).

$$\frac{t}{q_t} = \frac{t}{k_2 q_e^2} + \frac{t}{q_e} \quad (2)$$

The Elovich kinetic model is presented in Eq. (3).

$$q_t = b + a \ln t \quad (3)$$

where a and b are the Elovich constants.

Lastly, the intra-particle diffusion kinetic rate (k_i) from the intra-particle diffusion kinetic model was explained by the Weber-Morris model using Eq. (4):

$$q_t = k_i t^{0.5} + C \quad (4)$$

The ratio of adsorbates and adsorbents were studied using various isotherm methods. The Langmuir and Freundlich isotherms describe a monolayer of adsorbate on the and multilayer adsorbate on the adsorbent, respectively. The Langmuir and Freundlich equations are shown in Eqs. (5) and (6), respectively.

$$\frac{C_e}{q_e} = \frac{1}{q_{max} k_L} + \frac{C_e}{q_{max}} \quad (5)$$

$$q_e = K_F C_e^{1/n} \quad (6)$$

where q_{max} is the maximum adsorption capacity of adsorbents (mg • g^{-1}) and K_L and K_F represent the Langmuir adsorption constant (L • mg^{-1}) and Freundlich adsorption constant (mg • g^{-1}), respectively. The values of K_L and q_{max} are obtained from the intercept and slope of the linear plot of C_e versus C_e/q_e. In addition, n and K_F can be calculated from the slope and intercept of the linear plot of $\ln(C_e)$ against $\ln(q_e)$.

Table 1
Surface area and zeta potential of the adsorbents used in this study.

Adsorbents	Supplier	Country	Particle size by supplier	Surface area (m^2 • g^{-1})	Zeta potential (mV) at pH 5.5
h-BN-i	Tanyun Chemical	China	8~12 μm	10.8	−28.5
h-BN-ii	US Resesearch Nanomaterials	USA	70~80 nm	38.2	−34.0
h-BN-iii	skyspring	USA	~500 nm	49.3	−35.8
h-BN-iv	Naongrafi	Germany	65~75 nm	57.6	−36.3
h-BN-v	US Resesearch Nanomaterials	USA	~500 nm	30.9	−40.2

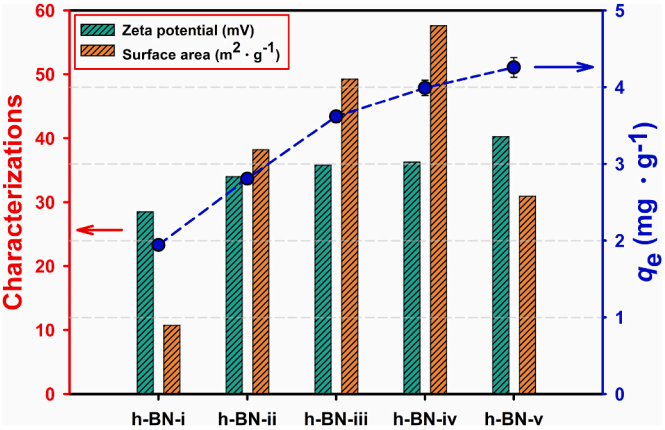


Fig. 1. Comparison of five kinds of h-BN for the removal of chromium in terms of surface area and charge (Experimental condition: 10 mg • L^{-1} Cr, 50 mg • L^{-1} Na, 50 mg • L^{-1} Ca, and 750 mg • L^{-1} h-BN at pH 5.5 with 4 h exposure time).

3. Results and discussion

3.1. Optimal h-BN for removal of chromium and its characterization

The adsorption performance of target elements is highly related to physico-chemical properties of the adsorbents (Jun et al., 2021). In this study, five different commercial h-BNs were utilized as adsorbents for the treatment of Cr in model groundwater. Table 1 summarizes general information of the five h-BNs and their surface area and zeta potential.

Fig. 1 provides a comparison of the five kinds of h-BN for the removal of Cr in terms of surface area and charge. Their adsorption performance decreased in the following order: h-BN-v > h-BN-iv > h-BN-iii > h-BN-ii > h-BN-i. Judging from the correlation coefficient between characterizations and q_e, surface charge (R^2 = 0.9168) was a more important factor compared to surface area (R^2 = 0.4809). This result is consistent with a previous study, which focused on the removal of lead by a metal-organic framework (MOF) and graphene oxide (GO) (Jun et al., 2019b). Specifically, the MOF, which has larger surface area and lower surface charge, showed a smaller q_e value than GO, which has smaller surface area and higher surface charge. Thus, electrostatic attraction by surface charge is the main adsorption mechanism to remove target heavy metals by h-BN. Based on having the highest q_e, h-BN-v was utilized in further performance tests as an optimal h-BN hereafter.

The surface charge of the optimized h-BN was measured by electrophoresis equipment, as shown in Fig. 2(a). The isoelectric point of h-BN was about 3.5, considering zeta potential values from pH 2 to pH 7.

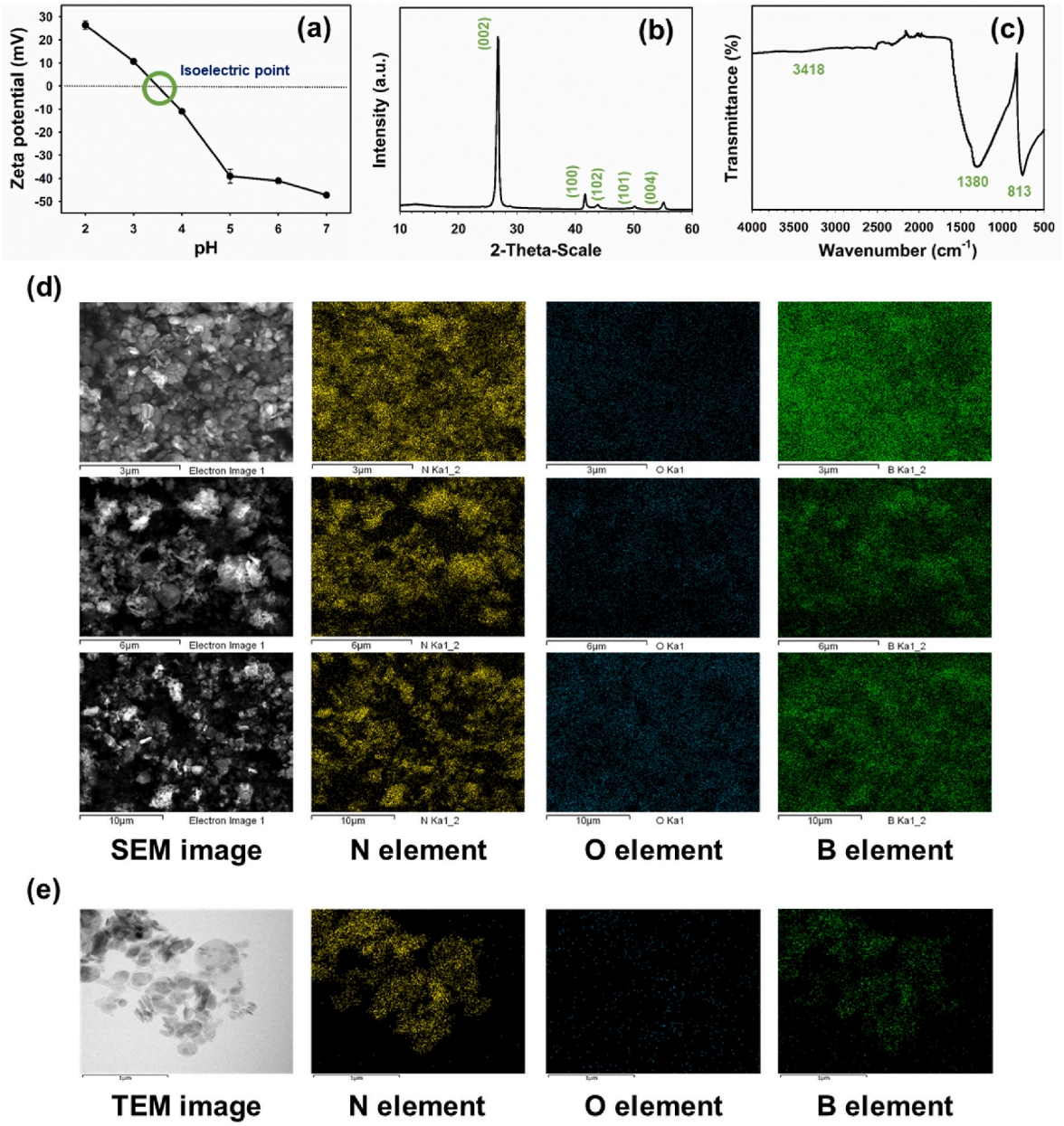


Fig. 2. Characterizations to clarify physico-chemical properties of the optimized h-BN: (a) zeta potential, (b) XRD, (c) FTIR, (d) SEM-EDS, and (e) TEM-EDS.

In order to clarify the. effect of solution pH on adsorption performance, we conducted four kinds of experiments (Experimental conditions: 10 mg • L^{-1} Cr(III) and 750 mg • L^{-1} h-BN at pH 2.5, 3.5, 4.5, and 5.5). Adsorption performance (q_e) increased with increasing solution pH as follows: 0.1 mg • g^{-1} at pH 2.5 < 0.7 mg • g^{-1} at pH 3.5 < 2.5 mg • g^{-1} at pH 4.5 < 4.2 mg • g^{-1} at pH 5.5. This result is in good agreement with the interpretation in Fig. 1; surface charge is the most important factor to determine adsorption performance for the removal of heavy metals (Zhao et al., 2021). The crystallinity and chemical bonds of h-BN are summarized in Fig. 2(b) and (c), respectively. The experimental results related to XRD and FTIR closely matched those of h-BN-based adsorbents previously reported elsewhere (Liu et al., 2019a; Oh et al., 2019; Li et al., 2020; Wang et al., 2020; Jun et al., 2024). In the case of XRD, the main diffraction peaks of the optimized h-BN were very similar with previous studies, based on the fact that the peaks were confirmed at (i) 26.7 (002), (ii) 41.7 (100), (iii) 43.9 (101), (iv) 50.2 (102), and (v) 55.1° (004), which represent crystal planes due to the hexagonal symmetry structure, considering JCPDS [34–0421]. Meanwhile, in the case of chemical bonds of h-BN, we confirmed two sharp peaks at ~1400 and 800 cm^{-1}, corresponding to in-plane stretching vibration of B–N and out-of-plane bending vibration of B–N–B bonds, respectively. In other words, the chemical bonds of h-BN were completely matched previously published h-BN-based adsorbents, as mentioned above. Lastly, Fig. 2(d) and (e) exhibit the morphology and elemental information of the h-BN, which were measured by SEM and TEM-EDS, respectively. The h-BN used in this study mainly consisted of N, O, and B elements; the adsorption mechanisms are further discussed in Section 3.3, based on elemental analyses via both FTIR and XPS techniques.

3.2. Adsorption and desorption properties of Cr(III) under different environmental conditions

3.2.1. Kinetic study

The effect of exposure time range from 0 to 1440 min (24 h) on the adsorption of Cr(III) by h-BN was evaluated for an adsorption kinetic study, as shown in Fig. 3. Most adsorption of Cr(III) by h-BN proceeded

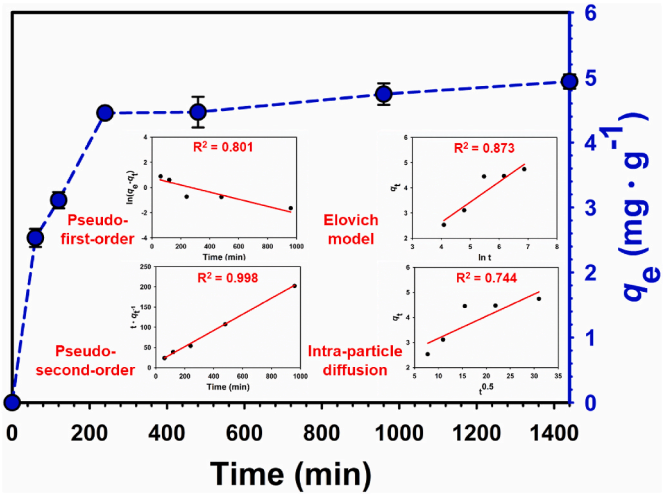


Fig. 3. Kinetic study of Cr(III) adsorption by h-BN with increasing exposure time. The inset figures exhibit several kinetic models to investigate the mechanism of Cr(III) adsorption by h-BN (Experimental condition: 10 mg • L^{-1} Cr, 50 mg • L^{-1} Na, 50 mg • L^{-1} Ca, and 750 mg • L^{-1} h-BN at pH 5.5 from 0 to 24 h exposure time).

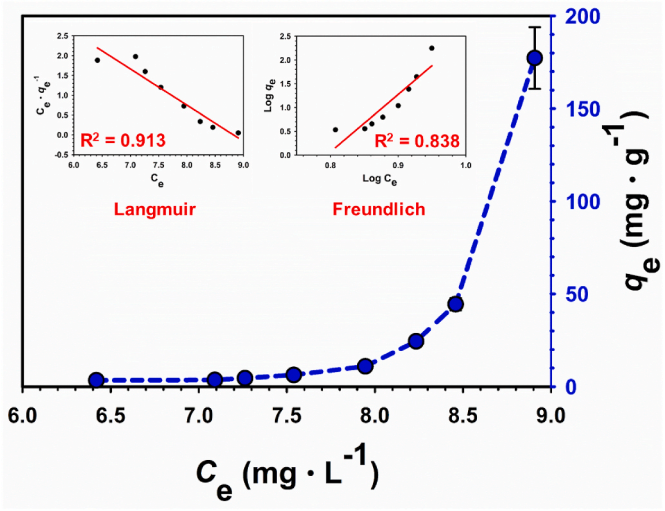


Fig. 4. Isotherm study of Cr(III) adsorption by h-BN with increasing C_e. The inset figures exhibit two isotherm models to investigate the mechanism of Cr (III) adsorption by h-BN (Experimental condition: 10 mg • L^{-1} Cr, 50 mg • L^{-1} Na, 50 mg • L^{-1} Ca, and 10–750 mg • L^{-1} h-BN at pH 5.5 with 4 h exposure time).

within 4 h exposure time, followed by a slight increase until 24 h exposure time. This could be explained by a gradual decrease of relatively vacant sites of the adsorbent toward target elements until reaching the equilibrium state (Oh et al., 2019; Kumar et al., 2020). Thus, from a practical perspective, 4 h exposure time was selected as a further experimental condition. We also evaluated four kinetic models, pseudo-1st-order, pseudo-2nd-order, Elovich model, and intra-particle diffusion models, in order to clarify the adsorption mechanism. Among them, the pseudo-2nd-order kinetic model best explained the adsorption of Cr(III) by h-BN, on the basis of having the highest correlation coefficient, and this is in good agreement with other kinetic results assessing the treatment of heavy metals by h-BN-based adsorbents (Peng et al., 2018; Bangari et al., 2019, 2020; Liu et al., 2019a, 2019b; Li et al., 2020). That is, main adsorption mechanism in the kinetic study was the chemisorption process between surface of h-BN and Cr(III) via electrostatic interactions.

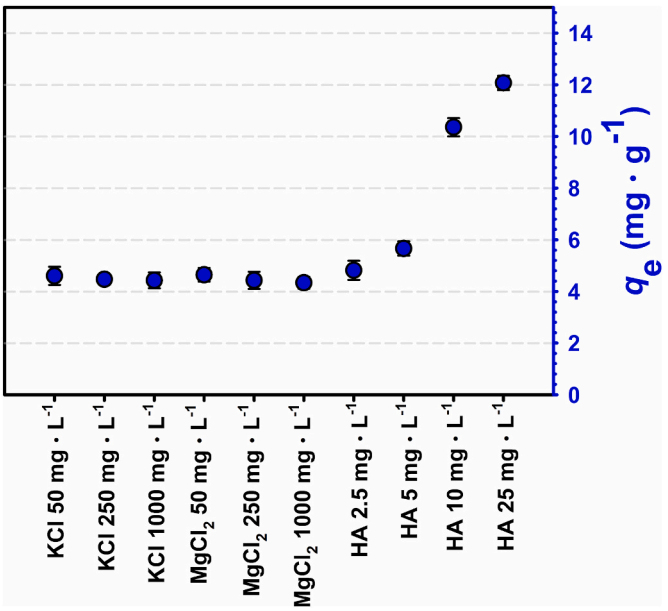


Fig. 5. Effect of background cations and humic acids on Cr(III) adsorption by h-BN (Experimental condition: 10 mg • L^{-1} Cr, 50 mg • L^{-1} Na, 50 mg • L^{-1} Ca, and 750 mg • L^{-1} h-BN at pH 5.5 with 4 h exposure time).

3.2.2. *Isotherm study*

The ratio of adsorbates and adsorbents is one of the critical factors to determine the mass transfer rate between adsorbates and adsorbents (Huang et al., 2016; Jun et al., 2020a; Chen et al., 2022). The adsorption isotherm was therefore confirmed by the effect of the ratio of adsorbates and adsorbents from 1:1 to 1:125 on the q_e, as shown in Fig. 4. The q_e continuously increased as the ratio of adsorbates and adsorbents decreased from 1:125 to 1:1 (or increasing C_e), considering the decrease of relatively vacant sites of h-BN toward Cr(III) (Oh et al., 2019; Kumar et al., 2020). The Langmuir and Freundlich models were utilized to perform an isotherm study of Cr(III) adsorption by h-BN. The Langmuir model, which assumes homogeneous as well as monolayer surface adsorption between adsorbate and adsorbent, could better explain the isotherm model in this study, according to the inset figure in Fig. 4. The correlation coefficient of the Langmuir model ($R^2 = 0.913$) was higher than that of the Freundlich model ($R^2 = 0.838$), which assumes heterogeneous as well as multilayer surface adsorption between adsorbate and adsorbent. These results are consistent with previous reports on the removal of heavy metals by the Langmuir model (Li et al., 2013, 2017; Peng et al., 2018; Wang et al., 2018, 2020; Bangari et al., 2019; Liu et al., 2019a, 2019b).

3.2.3. *Effect of background ions and humic acids on adsorption*

The influences of background ions and HA on q_e were assessed to study the adsorption mechanism of Cr(III) by h-BN, as shown in Fig. 5. In the case of background ions with different ionic strength, both the decrease of the surface charge density and the interference of co-ions contribute to the adsorption performance (Tan et al., 2015; Chu et al., 2017; Karthikeyan et al., 2020). An investigation of Cr(III) adsorption with co-existing ions (i.e., K and Mg) was then conducted using three different ionic strengths, from 50 to 1000 mg • L^{-1}, considering common ions in ground water (Cruz and Andrade, 2015; Kovalenko et al., 2021; Shiyan et al., 2022; Hansson et al., 2023). Notably, the adsorption performance was negligibly affected in the presence of co-ions; thus, h-BN could be utilized for the treatment of Cr(III) in various types of groundwater.

Fig. 5 summarizes the effect of the presence of HA on q_e of Cr(III) by h-BN. The adsorption performance of Cr(III) gradually increased with HA concentrations from 2.5 to 25 mg • L^{-1}. Notably, HA consists of

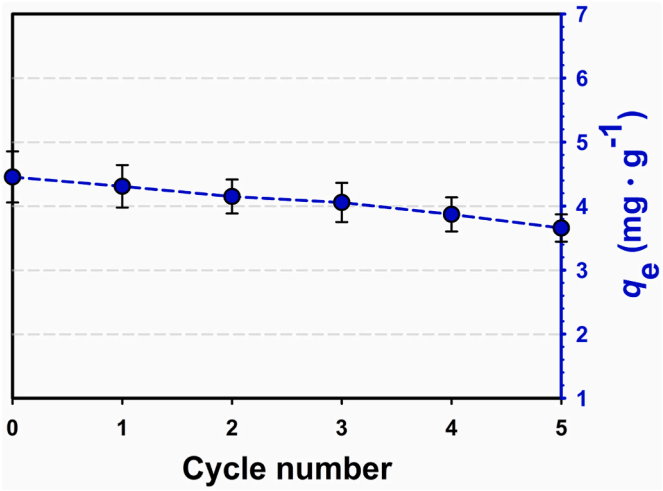


Fig. 6. Sequential desorption properties of h-BN (Experimental condition: 10 mg • L^{-1} Cr, 50 mg • L^{-1} Na, 50 mg • L^{-1} Ca, and 750 mg • L^{-1} h-BN at pH 5.5 with 4 h exposure time).

plentiful aromatic rings with carboxylic acids and thus acts as multi-valent anions. In other words, HA can capture Cr(III) via electrostatic attraction. Furthermore, there exist hydrophobic interactions between HA and h-BN, which promotes an increase q_e of Cr(III) by both HA and h-BN. Interestingly, q_e of Cr(III) by both HA and h-BN increased until 500 mg • g^{-1} in an extreme case (experimental conditions: 10 mg • L^{-1} Cr (III), 25 mg • L^{-1} HA, and 10 mg • L^{-1} h-BN at pH 5.5). The adsorption mechanism of Cr(III) by h-BN considering the experimental results is clarified by both FTIR and XPS characterizations in Section 3.3 below.

3.2.4. *Reusability testing*

A reusable property of h-BN is required for actual application to wastewater treatment. In order to confirm the reusability of h-BN, 0.1 M HCl (~pH 1) with 1 h contact time was applied to desorb Cr(III) from used h-BN, because the isoelectric point of the adsorbent was ~pH 3.5 [Fig. 2(a)]. Fig. 6 summarizes the sequential desorption properties of h-BN during five adsorption-desorption cycles. The q_e values of Cr(III) during five cycles were changed as follows: (i) 4.3 mg • g^{-1}, (ii) 4.1 mg • g^{-1}, (iii) 4.0 mg • g^{-1}, (iv) 3.9 mg • g^{-1}, and (v) 3.7 mg • g^{-1}. That is, the slight decrease of the reusability within five cycles could be explained by (i) the loss of the h-BN during recovery and (ii) minimal residual Cr(III) on h-BN. These outcomes are consistent with previous reports (Liu et al., 2019a, 2019b; Han et al., 2020).

3.3. *Plausible adsorption mechanism between h-BN and Cr(III)*

A plausible mechanism of Cr(III) adsorption by h-BN was clarified by FTIR spectra and XPS elemental results, as shown in Fig. 7. The main peaks of h-BN's FTIR spectra consist of (i) B–N–B bending vibration at

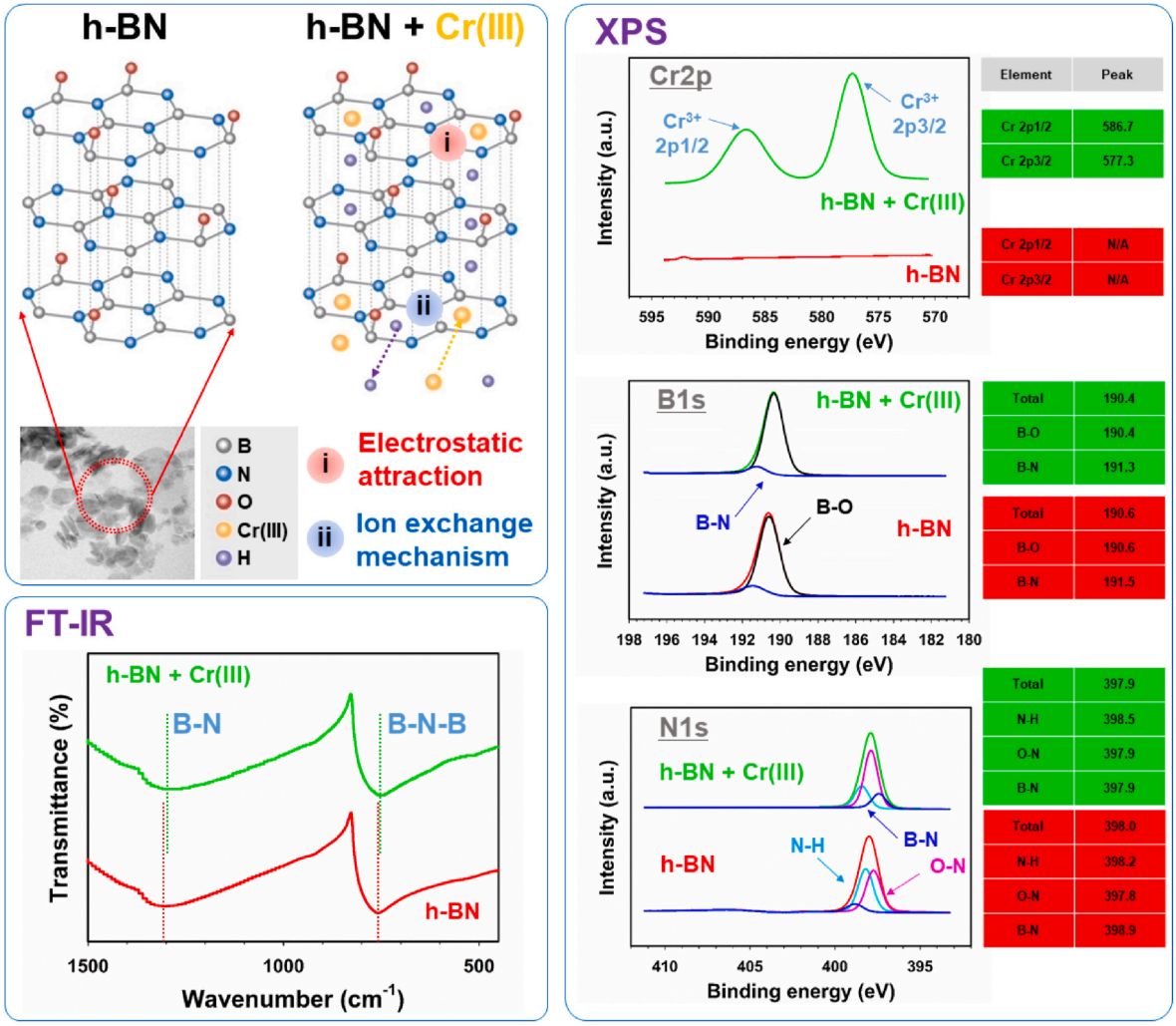


Fig. 7. Plausible mechanism of Cr(III) adsorption by h-BN through FTIR and XPS results.

Table 2
Comparison of adsorption performances of chromium ion by h-BN-based materials.

Adsorbent	Surface area ($m^2 \bullet g^{-1}$)	Experimental conditions	q_e or q_m ($mg \bullet g^{-1}$)	Environmental factors	Ref.
h-BN	31	$C_o = 10$ mg L^{-1} *Cr(III)* $C_o = 10$ mg L^{-1} Temp. = 298 K pH = 5.5	177.0 (q_m)	Cations (K^+ and Mg^{2+} from 50 to 1000 mg L^{-1}) Humic acids from 2.5 to 25 mg L^{-1}	This study
Activated BN	1104	$C_o = 52$ mg L^{-1} *Cr(III)* $C_o = 10$ mg L^{-1} Temp. = 303 K pH = 5.5	149.0 (q_m)	Solution temperature	Li et al. (2014)
Fluorinated activated BN	1250	$C_o = 52$ mg L^{-1} *Cr(III)* $C_o = 10$ mg L^{-1} Temp. = 303 pH = 5.5	387.0 (q_m)	Solution temperature	Li et al. (2014)
Amine-functionalized BN	342	$C_o = 200$ mg L^{-1} *Cr(VI)* $C_o = 20$ mg L^{-1} Temp. = 298 K pH = 2.0	83.4 (q_m)	Solution temperature Solution pH	Song et al. (2023)
h-BN-Fe_3O_4	105	$C_o = 200$ mg L^{-1} *Cr(VI)* $C_o = 20$ mg L^{-1} Temp. = 323 K pH = 3.0	208.6 (q_m)	Solution pH	Lawal Usman et al. (2022)
h-BN/$CdAl_2O_4$	N/A	$C_o = 500$ mg L^{-1} *Cr(VI)* $C_o = 15$ mg L^{-1} pH = 3.0	2.3 (q_e)	N/A	Kumar et al. (2020)
h-BN@5%Pani	264	$C_o = 1000$ mg L^{-1} *Cr(VI)* $C_o = 100$ mg L^{-1} Temp. = 323 K pH = 4.0	133.4 (q_e)	Solution pH	Karthikeyan et al. (2020)
BN@ZVI	794	$C_o = 500$ mg L^{-1} *Cr(VI)* $C_o = 50$ mg L^{-1} Temp. = 298 K pH = 2.0	349.0 (q_e)	Anions (Cl^-, SO_4^{2-}, $H_2PO_4^-$ And CO_3^{2-})	Chen et al. (2022)
Activated BN	606	$C_o = 1000$ mg L^{-1} *Cr(III)* $C_o = 40$ mg L^{-1} Temp. = 298 K pH = 6.0	423.2 (q_m)	N/A	Li et al. (2017)
BN nanocage	N/A	*Computational calculation*	N/A	N/A	Waheed Kamran et al. (2023)
Activated BN	2078	*Cr(III)* $C_e = 50$ mg L^{-1} pH = 6.0	352.0 (q_m)	N/A	Li et al. (2013)

~800 cm^{-1}, (ii) B–N bending vibration at ~1400 cm^{-1}, and (iii) B–OH and B–NH_2 stretching vibration at ~3600 and ~3400 cm^{-1}, respectively (Liu et al., 2019b; Oh et al., 2019; Li et al., 2020). In this study, we clearly confirmed two main peaks of B–N–B and B–N bending vibration at ~800 cm^{-1} and ~1400 cm^{-1}, respectively, as seen in Fig. 2(c). Several studies have clarified peak changes of FTIR after the reaction between h-BN and heavy metals (Liu et al., 2019a, 2019b; Oh et al., 2019; Bangari et al., 2020; Li et al., 2020); the FTIR results in Fig. 7 also exhibited slight peak shifts of B–N–B and B–N bending vibration after the reaction between h-BN and Cr(III) due to its electrostatic complexation.

XPS analyses regarding Cr, B, and N elements were further carried out to confirm the adsorption mechanism between h-BN and Cr(III). First, Cr(III) 2p1/2 and 3/2 peaks at 586.7 and 577.3 eV newly appeared after the reaction between h-BN and Cr(III); thus, h-BN is chemically adsorbed Cr(III) via electrostatic attraction. Second, in the case of the B element, small shifts of B–O and B–N at 190.4 and 191.3 eV from 190.6 to 191.5, respectively, were observed. Likewise, the peak of total N element was also shifted from 398.0 to 397.9 eV due to chemisorption, considering previously reported results (Peng et al., 2018; Liu et al., 2019a; Li et al., 2020). Lastly, the peak of N–H was dramatically decreased by the adsorption of N and the target element, judging from deconvolution of N 1s before and after reaction between h-BN and Cr (III) (Peng et al., 2018). Based on the above explanation, high electrostatic attraction as well as the ion exchange mechanism between hydrogen and target element mainly accounted for the adsorption mechanism of Cr(III) by h-BN. Finally, Table 2 summarizes a comparison of q_e or q_m for chromium ion between this study and the previously-reported h-BN-based materials. In other words, h-BN-based materials are suitable for treatment of chromium ion in contaminated groundwater, judging from the excellent adsorption performances in the presence of various environmental factors (e.g., co-ions, HA, and so on).

4. Conclusions

Thus far, no comprehensive study of the adsorption of Cr(III) by h-BN under various experimental conditions such as exposure time, ratio of adsorbates and adsorbents, solution pH, background ions with different ionic strength, and the presence of HA in model contaminated groundwater has been conducted. Five forms of h-BN as an adsorbent were applied to treat Cr(III) from model contaminated groundwater in this study. Among them, the optimized h-BN was selected based on having the highest q_e due to its abundant negative surface charge. The optimized h-BN exhibited excellent maximum adsorption capacity (*i.e.*, 177 $mg \bullet g^{-1}$) when the concentrations of Cr(III) and h-BN were 10 and 10 $mg \bullet L^{-1}$, respectively. The adsorption performance of Cr(III) by h-BN was enhanced with increasing solution pH because of increasing negative surface charge. Subsequently, in terms of kinetic and isotherm studies, the adsorption mechanism of Cr(III) by h-BN tended to follow a pseudo-2nd-order kinetic model and Langmuir isotherm model, respectively. Meanwhile, we also confirmed there was a negligible change in the adsorption performance of Cr(III) by h-BN in the presence of co-ions varied from 50 to 1000 $mg \bullet L^{-1}$ (*i.e.*, K and Mg). The specific adsorption mechanism of Cr(III) by h-BN was clarified by FTIR and XPS characterizations, and electrostatic complexation and ion exchange were found to be the dominant adsorption mechanisms in this study. h-

BN presented good reusability, showing only a slight decrease in adsorption performance during five adsorption-desorption cycles. Finally, considering the experimental results using model Cr(III)-contaminated groundwater obtained in this study, including excellent adsorption performance and reusability, h-BN can be effectively applied to treat Cr(III)-contaminated groundwater containing several co-ions (e.g., K and Mg) and natural organic matters (e.g., HA).

CRediT authorship contribution statement

Byung-Moon Jun: Writing – original draft, Visualization, Validation, Methodology, Investigation, Formal analysis. **Deokhwan Kim:** Methodology, Investigation, Formal analysis, Data curation. **Jaegwan Shin:** Investigation, Formal analysis, Data curation. **Kangmin Chon:** Resources, Investigation. **Chanhyuk Park:** Writing – review & editing, Validation. **Hojung Rho:** Writing – review & editing, Validation, Resources, Funding acquisition, Conceptualization.

Declaration of competing interest

The authors declare that they have no known competing financial interests or personal relationships that could have appeared to influence the work reported in this paper.

Data availability

Data will be made available on request.

Acknowledgements

This work was supported by the National Research Foundation of Korea (NRF) and Commercialization Promotion Agency for R&D Outcomes (COMPA) grant funded by the Korea government (MSIT) (RS2023-00233235). This work was also supported by the National Research Council of Science and Technology (NST) grant funded by the Korea government (MSIT) (CCL23101-100).

References

Bangari, R.S., Singh, A.K., Namsani, S., Singh, J.K., Sinha, N., 2019. Magnetite-coated boron nitride nanosheets for the removal of arsenic(V) from water. ACS Appl. Mater. Interfaces 11, 19017–19028.

Bangari, R.S., Yadav, V.K., Singh, J.K., Sinha, N., 2020. Fe_3O_4-functionalized boron nitride nanosheets as novel adsorbents for removal of arsenic(III) from contaminated water. ACS Omega 5, 10301–10314.

Chen, T., Zhou, Z., Xu, S., Wang, H., Lu, W., 2015. Adsorption behavior comparison of trivalent and hexavalent chromium on biochar derived from municipal sludge. Bioresour. Technol. 190, 388–394.

Chen, W., Xu, X., Cui, J., Zhou, Z., Yao, Y., 2022. Porous boron nitride intercalated zero-valent iron particles for highly efficient elimination of organic contaminants and Cr (VI). Chemosphere 306, 135501.

Chu, K.H., Fathizadeh, M., Yu, M., Flora, J.R.V., Jang, A., Jang, M., Park, C.M., Yoo, S.S., Her, N., Yoon, Y., 2017. Evaluation of removal mechanisms in a graphene oxide-coated ceramic ultrafiltration membrane for retention of natural organic matter, pharmaceuticals, and inorganic salts. ACS Appl. Mater. Interfaces 9, 40369–40377.

Crini, G., Lichtfouse, E., 2019. Advantages and disadvantages of techniques used for wastewater treatment. Environ. Chem. Lett. 17, 145–155.

Cruz, J.V., Andrade, C., 2015. Natural background groundwater composition in the Azores archipelago (Portugal): a hydrogeochemical study and threshold value determination. Sci. Total Environ. 520, 127–135.

Gonsalves, O.S., Nemade, P.R., 2024. Ultrafast adsorption of hexavalent chromium from aqueous effluents using covalent triazine frameworks. Chemosphere 351, 141246.

Hailemariam, RH, Choi, J-S, Damtie, MM, Rho, H, Park, K-D, Lee, J, et al., 2022. Enhancing performances of polyamide thin film composite membranes via co-solvent assisted interfacial polymerization. Desalination 524, 115481.

Han, F., Zong, Y., Jassby, D., Wang, J., Tian, J., 2020. The interactions and adsorption mechanisms of ternary heavy metals on boron nitride. Environ. Res. 183, 109240.

Hansson, N.L., Saleh, M., Tam, P.L., Holgersson, S., Spahiu, K., Ekberg, C., 2023. Influence of groundwater composition on the reductive precipitation of U(VI) on corroding iron foil surfaces. J. Nucl. Mater. 577, 154324.

Hashem, M.A., Mim, M.W., Noshin, N., Maoya, M., 2024a. Chromium adsorption capacity from tannery wastewater on thermally activated adsorbent derived from kitchen waste biomass. Clean. Water 1, 100001.

Hashem, M.A., Nayeen, J., Tanvir Hossain, M., Mukimujjaman Miem, M., 2024b. Chromium adsorption on thermally activated adsorbent equipped from waste biomass. Waste Manag. Bull. 2, 239–249.

Huang, S., Ma, C., Liao, Y., Min, C., Du, P., Zhu, Y., Jiang, Y., 2016. Superb adsorption capacity and mechanism of poly(1-amino-5-chloroanthraquinone) nanofibrils for lead and trivalent chromium ions. React. Funct. Polym. 106, 76–85.

Jun, B.-M., Chae, S.H., Kim, D., Jung, J.-Y., Kim, T.-J., Nam, S.-N., Yoon, Y., Park, C., Rho, H., 2024. Adsorption of uranyl ion on hexagonal boron nitride for remediation of real U-contaminated soil and its interpretation using random forest. J. Hazard Mater. 469, 134072.

Jun, B.-M., Hwang, H.S., Heo, J., Han, J., Jang, M., Sohn, J., Park, C.M., Yoon, Y., 2019a. Removal of selected endocrine-disrupting compounds using Al-based metal organic framework: performance and mechanism of competitive adsorption. J. Ind. Eng. Chem. 79, 345–352.

Jun, B.-M., Jang, M., Park, C.M., Han, J., Yoon, Y., 2020a. Selective adsorption of Cs^+ by MXene ($Ti_3C_2T_x$) from model low-level radioactive wastewater. Nucl. Eng. Technol. 52, 1201–1207.

Jun, B.-M., Kim, S., Kim, Y., Her, N., Heo, J., Han, J., Jang, M., Park, C.M., Yoon, Y., 2019b. Comprehensive evaluation on removal of lead by graphene oxide and metal organic framework. Chemosphere 231, 82–92.

Jun, B.-M., Lee, H.-K., Park, S., Kim, T.-J., 2021. Purification of uranium-contaminated radioactive water by adsorption: a review on adsorbent materials. Sep. Purif. Technol. 278, 119675.

Jun, B.-M., Park, C.M., Heo, J., Yoon, Y., 2020b. Adsorption of Ba^{2+} and Sr^{2+} on $Ti_3C_2T_x$ MXene in model fracking wastewater. J. Environ. Manage. 256, 109940.

Karthikeyan, P., Elanchezhiyan, S.S., Preethi, J., Meenakshi, S., Park, C.M., 2020. Mechanistic performance of polyaniline-substituted hexagonal boron nitride composite as a highly efficient adsorbent for the removal of phosphate, nitrate, and hexavalent chromium ions from an aqueous environment. Appl. Surf. Sci. 511, 145543.

khan, F., A N, Din, I.U., Saeed, T., Alotaibi, M.A., Alharthi, A.I., Habib, A., Malik, T., 2021. Synthesis, characterization and adsorption studies of h-BN crystal for efficient removal of Cd^{2+} from aqueous solution. Ceram. Int. 47, 4749–4757.

Kovalenko, I.O., Panasiuk, M.I., Skorbun, A.D., Sosonna, N.V., Ojovan, M.I., Shevchenko, O.L., Onyshchenko, I.P., 2021. Correlation between chemical composition and ^{90}Sr concentrations in groundwater of the Chornobyl NPP industrial site. J. Environ. Radioact. 240, 106756.

Kumar, P.A., Ray, M., Chakraborty, S., 2009. Adsorption behaviour of trivalent chromium on amine-based polymer aniline formaldehyde condensate. Chem. Eng. J. 149, 340–347.

Kumar, R., Barakat, M.A., Alseroury, F.A., Al-Mur, B.A., Taleb, M.A., 2020. Experimental design and data on the adsorption and photocatalytic properties of boron nitride/cadmium aluminate composite for Cr(VI) and cefoxitin sodium antibiotic. Data Br 28, 105051.

Lawal Usman, U., Kumar Allam, B., Bahadur Singh, N., Banerjee, S., 2022. Adsorptive removal of Cr(VI) from wastewater by hexagonal boron nitride-magnetite nanocomposites: kinetics, mechanism and LCA analysis. J. Mol. Liq. 354, 118833.

Lee, H.-K., Jun, B.-M., Kim, I., Eun, H.-C., Park, W., Jang, W.H., Kim, T.-J., Nam, S.-N., Yoon, Y., Park, S., 2023. Design and applicability of a water recycling system to treat wastewater generated from real uranium-contaminated soil. Chem. Eng. J. 472, 144927.

Li, J., Jin, P., Dai, W., Wang, C., Li, R., Wu, T., Tang, C., 2017. Excellent performance for water purification achieved by activated porous boron nitride nanosheets. Mater. Chem. Phys. 196, 186–193.

Li, J., Jin, P., Tang, C., 2014. Cr(III) adsorption by fluorinated activated boron nitride: a combined experimental and theoretical investigation. RSC Adv. 4, 14815–14821.

Li, J., Xiao, X., Xu, X., Lin, J., Huang, Y., Xue, Y., Jin, P., Zou, J., Tang, C., 2013. Activated boron nitride as an effective adsorbent for metal ions and organic pollutants. Sci. Rep. 3.

Li, L., Chang, K., Fang, P., Du, K., Chen, C., Zhou, S., Shen, C., Linghu, W., Sheng, G., Hayat, T., Guo, X., 2020. Highly efficient scavenging of Ni(II) by porous hexagonal boron nitride: kinetics, thermodynamics and mechanism aspects. Appl. Surf. Sci. 521, 146373.

Li, Q., Liu, Y., Yu, X., Li, L., Zhang, X., Lu, Z., Lin, J., Yang, X., Huang, Y., 2018. Removal of Cr(III)/Cr(VI) from wastewater using defective porous boron nitride: a DFT study. Inorg. Chem. Front. 5, 1933–1940.

Liu, G., Cui, C., Jiang, L., Gao, H., Gao, J., 2021. Visible light-induced hydrogels towards reversible adsorption and desorption based on trivalent chromium in aqueous solution. React. Funct. Polym. 163, 104886.

Liu, T., Li, Y.-L., He, J.-Y., Hu, Y., Wang, C.-M., Zhang, K.-S., Huang, X.-J., Kong, L.-T., Liu, J.-H., 2019a. Porous boron nitride nanoribbons with large width as superior adsorbents for rapid removal of cadmium and copper ions from water. New J. Chem. 43, 3280–3290.

Liu, T., Li, Y., He, J., Zhang, K., Hu, Y., Chen, X., Wang, C., Huang, X., Kong, L., Liu, J., 2019b. Few-layered boron nitride nanosheets as superior adsorbents for the rapid removal of lead ions from water. J. Mater. Sci. 54, 5366–5380.

Liu, W., Yu, Y., 2021. Removal of recalcitrant trivalent chromium complexes from industrial wastewater under strict discharge standards. Environ. Technol. Innov. 23, 101644.

Lohrentz, L., Bhaumik, M., Brink, H.G., 2023. High-capacity adsorption of hexavalent chromium by a polyaniline-Ni(0) nanocomposite adsorbent: expanding the Langmuir-Hinshelwood kinetic model. J. Mol. Liq. 389, 122931.

Manna, M., Sen, S., 2024. A mechanistic evaluation for total removal of toxic hexavalent and trivalent chromium from water by oxygen vacancy-engineered nanocomposite. J. Environ. Chem. Eng. 12, 111755.

Monga, A., Fulke, A.B., Dasgupta, D., 2022. Recent developments in essentiality of trivalent chromium and toxicity of hexavalent chromium: implications on human health and remediation strategies. J. Hazard. Mater. Adv. 7, 100113.
Oh, W.-D., Lee, M.G.H., Chanaka Udayanga, W.D., Veksha, A., Bao, Y., Giannis, A., Lim, J.-W., Lisak, G., 2019. Insights into the single and binary adsorption of copper (II) and nickel(II) on hexagonal boron nitride: performance and mechanistic studies. J. Environ. Chem. Eng. 7, 102872.
Padervand, M., Lichtfouse, E., Robert, D., Wang, C., 2020. Removal of microplastics from the environment. A review. Environ. Chem. Lett. 18, 807–828.
Peng, D., Jiang, W., Li, F.-F., Zhang, L., Liang, R.-P., Qiu, J.-D., 2018. One-pot synthesis of boron carbon nitride nanosheets for facile and efficient heavy metal ions removal. ACS Sustain. Chem. Eng. 6, 11685–11694.
Petrović, R., Lazarević, S., Janković-Častvan, I., Matić, T., Milivojević, M., Milošević, D., Veljović, Đ., 2023. Removal of trivalent chromium from aqueous solutions by natural clays: valorization of saturated adsorbents as raw materials in ceramic manufacturing. Appl. Clay Sci. 231, 106747.
Shiyan, L.N., Machekhina, K.I., Frantcuzskaia, E.O., 2022. Groundwater sources in the West Siberian region: chemical composition, analysis, and water treatment technologies. Clean. Eng. Technol. 7, 100441.
Song, Z., Guo, K., Bai, W., Tang, C., 2023. Adsorption and removal of Cr(VI) from aqueous solution with amine-functionalized porous boron nitride. J. Solid State Chem. 317, 123720.
Tan, L., Liu, Q., Jing, X., Liu, J., Song, D., Hu, S., Liu, L., Wang, J., 2015. Removal of uranium(VI) ions from aqueous solution by magnetic cobalt ferrite/multiwalled carbon nanotubes composites. Chem. Eng. J. 273, 307–315.
Waheed Kamran, A., Zahoor, M., Ali, H., Khan, S., Abu-Farsakh, H., Ali, S., 2023. Chromate ions chemisorption over the exterior surface of pristine boron nitride ($B_{12}N_{12}$) nanocage: a computational study. Inorg. Chem. Commun. 148, 110370.
Wang, H., Wang, W., Wang, H., Zhang, F., Li, Y., Fu, Z., 2018. Urchin-like boron nitride hierarchical structure assembled by nanotubes-nanosheets for effective removal of heavy metal ions. Ceram. Int. 44, 12216–12224.
Wang, J., Zhao, S., Ling, Z., Zhou, T., Liu, P., Li, X., 2021. Enhanced removal of trivalent chromium from leather wastewater using engineered bacteria immobilized on magnetic pellets. Sci. Total Environ. 775, 145647.
Wang, M., Bai, Y., Zhang, B., Zhong, B., Yu, Y., Zhang, J., Huang, X., Wen, G., 2019. Large scale fabrication of porous boron nitride microrods with tunable pore size for superior copper (II) ion adsorption. Ceram. Int. 45, 6684–6692.
Wang, S., Jia, F., Kumar, P., Zhou, A., Hu, L., Shao, X., Wang, X., Sun, Y., Yin, G., Liu, B., 2020. Hierarchical porous boron nitride nanosheets with versatile adsorption for water treatment. Colloids Surf. A: Physicochem. Eng. Asp. 598, 124865.
Yang, S., Li, L., Pei, Z., Li, C., Lv, J., Xie, J., Wen, B., Zhang, S., 2014. Adsorption kinetics, isotherms and thermodynamics of Cr(III) on graphene oxide. Colloids Surf. A: Physicochem. Eng. Asp. 457, 100–106.
Zhao, Z., Lanzarini-Lopes, M., Westerhoff, E., Long, X., Rho, H., Bi, Y., Ling, L., Westerhoff, P., 2021. Evanescent wave interactions with nanoparticles on optical fiber modulate side emission of germicidal ultraviolet light. Environ. Sci. Nano 8 (9), 2441–2452.